

AD-A275 165

2. REPORT DATE  
December 28, 19933. REPORT TYPE AND DATES COVERED  
Reprint

②

4. TITLE AND SUBTITLE  
SPECTROSCOPIC AND PHOTOMETRIC OBSERVATIONS OF A FIVE-  
MAGNITUDE FLARE EVENT ON UV CETI5. FUNDING NUMBERS  
PE 61102F  
PR 2311  
TA G3  
WU 276. AUTHOR(S)  
Erik L. E. Eason\*, M.S. Giampapa\*\*, R.R. Radick,  
S.P. Worden#, E.K. Hege##7. PERFORMING ORGANIZATION NAME(S) AND ADDRESS(ES)  
Phillips Lab/GPSS  
29 Randolph Road  
Hanscom AFB, MA 01731-30108. PERFORMING ORGANIZATION  
REPORT NUMBER  
PL-TR-93-2258OPTIC  
SELECTE  
JAN 9 1994  
SAD

9. SPONSORING MONITORING AGENCY NAME(S) AND ADDRESS(ES)

10. SPONSORING MONITORING  
AGENCY REPORT NUMBER11. SUPPLEMENTARY NOTES\*The Aerospace Corp, Los Angeles, CA 90009-2957, \*\*National Solar  
Observatory, National Astronomy Observatories, Tucson AZ 85726 #National Space  
Council, Executive Office of the President, Washington, DC 20301-7100 ##Steward  
Observatory, University of Arizona, Tucson AZ 85721 - Reprinted from The  
Astronomical Journal, Volume 104, Number 3, September 199212. DISTRIBUTION STATEMENT  
Approved for public release; Distribution unlimited13. ABSTRACT  
We present optical observations of a 5 mag flare in the U band on UV Ceti (dM5.6e) at both high spectral and temporal resolutions. A strong violet continuum is seen which cannot be reproduced solely with a thermal bremsstrahlung spectrum. The energy emitted by the flare in the U band is approximately  $5.0 \times 10^{31}$  ergs. The corresponding total flare energy in white light is estimated to be  $1.2 \times 10^{32}$  ergs. This estimate, combined with the 700 s duration of the U-band event, yields an average white-light flare luminosity which is  $\sim 3\%$  of the quiescent stellar bolometric luminosity. The Balmer series is evident out to H14, and the flux of H $\delta$  nearly equals H $\gamma$  at maximum light. Significantly, Ca II H and K initially declined in total strength by a factor of 3 before rising above the flare continuum, thus indicating a rapid and significant disturbance of the lower chromosphere. Strong H $\alpha$  wings appeared after the impulsive phase. Stark broadening was not entirely satisfactory at fitting the wing profile; however, a highly broadened Doppler profile ( $\Delta\lambda_D = 3.5 \text{ \AA}$ ) which is blueshifted by  $\Delta\lambda_m = -1.5 \text{ \AA}$  fits extremely well. We interpret this as evidence for chromospheric material with a microturbulent velocity of  $150 \text{ km s}^{-1}$  that is also rising with a velocity component in the line of sight of about  $70 \text{ km s}^{-1}$  or, alternatively, the superposition of several discrete chromospheric ejections. The width and blueshifts persisted unchanged for 40 min before observing terminated. A discernible central reversal is present in both the quiescent H $\alpha$  profile and, significantly, in the flare profile following the impulsive phase. These observations suggest that the site of H $\alpha$  flare emission is not necessarily associated with a compact, high pressure region. Rather, the flare-enhanced line emission arises from large flare volumes that are, in turn, a distinguishing feature of stellar flares of this magnitude.14. SUBJECT TERMS  
Photometry, Stellar Activity, Stellar Flares, Spectroscopy15. NUMBER OF PAGES  
13  
16. PRICE CODE17. SECURITY CLASSIFICATION  
OF REPORT  
UNCLASSIFIED18. SECURITY CLASSIFICATION  
OF THIS PAGE  
UNCLASSIFIED19. SECURITY CLASSIFICATION  
OF ABSTRACT  
UNCLASSIFIED20. LIMITATION OF ABSTRACT  
SAR

SPECTROSCOPIC AND PHOTOMETRIC OBSERVATIONS OF A FIVE-MAGNITUDE  
FLARE EVENT ON UV CETI

ERIK L. E. EASON

The Aerospace Corporation, Los Angeles, California 90009-2957

M. S. GIAMPAPA

National Solar Observatory, National Optical Astronomy Observatories,<sup>1</sup> Tucson, Arizona 85726R. R. RADICK<sup>2</sup>

Phillips Laboratory/Solar Research Branch, National Solar Observatory, Sunspot, New Mexico 88349

S. P. WORDEN<sup>2</sup>

National Space Council, Executive Office of the President, Washington, DC 20301-7100

E. K. HEGE

Steward Observatory, University of Arizona, Tucson, Arizona 85721

Received 31 October 1991; revised 12 May 1992

## ABSTRACT

We present optical observations of a 5 mag flare in the  $U$  band on UV Ceti (dM5.6e) at both high spectral and temporal resolutions. A strong violet continuum is seen which cannot be reproduced solely with a thermal bremsstrahlung spectrum. The energy emitted by the flare in the  $U$  band is approximately  $5.0 \times 10^{31}$  ergs. The corresponding total flare energy in white light is estimated to be  $1.2 \times 10^{32}$  ergs. This estimate, combined with the 700 s duration of the  $U$ -band event, yields an average white-light flare luminosity which is  $\sim 3\%$  of the quiescent stellar bolometric luminosity. The Balmer series is evident out to H14, and the flux of H $\delta$  nearly equals H $\gamma$  at maximum light. Significantly, Ca II H and K initially declined in total strength by a factor of 3 before rising above the flare continuum, thus indicating a rapid and significant disturbance of the lower chromosphere. Strong H $\alpha$  wings appeared after the impulsive phase. Stark broadening was not entirely satisfactory at fitting the wing profile; however, a highly broadened Doppler profile ( $\Delta\lambda_D = 3.5 \text{ \AA}$ ) which is blueshifted by  $\Delta\lambda_{bs} = -1.5 \text{ \AA}$  fits extremely well. We interpret this as evidence for chromospheric material with a microturbulent velocity of  $150 \text{ km s}^{-1}$  that is also rising with a velocity component in the line of sight of about  $70 \text{ km s}^{-1}$  or, alternatively, the superposition of several discrete chromospheric ejections. The width and blueshifts persisted unchanged for 40 min before observing terminated. A discernible central reversal is present in both the quiescent H $\alpha$  profile and, significantly, in the flare profile following the impulsive phase. These observations suggest that the site of H $\alpha$  flare emission is not necessarily associated with a compact, high pressure region. Rather, the flare-enhanced line emission arises from large flare volumes that are, in turn, a distinguishing feature of stellar flares of this magnitude.

## 1. INTRODUCTION

Flare stars are late-type emission-line main sequence stars which exhibit random and rapid increases in luminosity. All dwarf M stars thus far observed in the blue-visible and near ultraviolet emit Ca II H and K and Mg II h and k arising from their low to midchromospheres, respectively. However, only those with enhanced chromospheric and transition region densities emit H $\alpha$  (distinguishing dMe from dM) as well as a host of other optical and ultraviolet emission lines. There are several classes of stars that exhibit flaring behavior and related phenomena similar to solar magnetic activity. UV Ceti is the classic prototype of the

flare star. These flare stars are isolated star systems characterized by a wide range of flaring properties that include, for example, the frequency of flaring and the total flare energy. Reviews of the properties of flare stars are given by Kunkel (1975), Gershberg (1975), Mullan (1977), Gurzadyan (1980), Byrne & Rodonò (1983). Reviews of the properties of solar flares and/or stellar flares are presented by Svestka (1976), Sturrock (1980), Kane *et al.* (1983), Gondhalekar (1986), Haisch & Rodonò (1989), and Haisch *et al.* (1991).

The dMe stars are intrinsically faint and only the nearest are suitable for detailed study, and of these only marginally. Their faintness makes high resolution spectral observations difficult, and has precluded high temporal and spectral resolution observations combined, until the advent of solid state detectors. The vast majority of observations are in the form of broad-band photometry, usually with

<sup>1</sup>Operated by the Association of Universities for Research in Astronomy, Inc., under cooperative agreement with the National Science Foundation.

<sup>2</sup>Visiting Astronomer, Kitt Peak National Observatory.

94-01683  
590 41 1 46

Johnson *UBV* filters. The *U* band always shows a larger relative change than the *B* band, which always shows a larger relative change than the *V* band. The flare spectrum is "blue," due both to enhanced UV emission lines and a continuum suggestive of an optically thick, radiating plasma which is much hotter than the underlying M-dwarf photosphere. These properties are qualitatively similar to solar white light flares (c.f. Neidig 1989). Photometrically, flares are quite varied in temporal profile and color. However, they are traditionally divided into two categories (even though this belies their variety): "spike flares" typically reach peak intensity in less than a minute while "slow flares" take several minutes. Initially the decay toward quiescence is rapid, falling below half-maximum in several minutes. In most flares the rate of decay quite suddenly slows appreciably, and then can take several hours to relax fully to quiescence. Large flares, such as the one discussed herein, typically exhibit the superposition of slow and fast events (see Byrne 1983). This apparent superposition may be the result of several related flares, or a "wavelike" flaring in the stellar active regions. Solar white light flares show just such behavior (Neidig & Cliver 1983).

Optical spectroscopy reveals that a strong continuum rises to dominate the violet and blue region during maximum light (Worden 1983). The Balmer series (observed out to H14), Ca II H and K, and He I all rise with the continuum, but usually peak a few minutes afterwards (Giampapa 1983). The rapid decline of the continuum is responsible for the initial photometric decay, while the emission lines slowly return to quiescence (Bopp & Moffett 1973).

Haisch *et al.* (1981) observed several flares with the *International Ultraviolet Explorer (IUE)* satellite observatory. They time trailed the telescope giving a temporal resolution of 5<sup>m</sup>–10<sup>m</sup>, and alternated between the SWP (1150–2000 Å) and LWP (2000–3400 Å) cameras. Quite surprisingly neither the UV emission lines nor the UV continuum were significantly altered by the flares. The emission lines changed by less than a factor of two and no continuum enhancement was apparent, within an upper limit on both of  $5 \times 10^{-15} \text{ erg s}^{-1} \text{ cm}^{-2} \text{ Å}^{-1}$ . It had been anticipated that flare emission would have been observable from one or more of the following sources: bremsstrahlung from a  $10^7 \text{ K}$  plasma, recombination continuum converting x-ray photons into  $\lambda > 912 \text{ Å}$  photons (Mullan 1977; Mullan & Tarter 1977), and enhancement of transition region and chromospheric emission lines as these regions are heated by the flare. That the UV emission lines showed no significant enhancement is particularly surprising since their optical counterparts are observed in similar flares to change by factors of 5 or more.

Haisch (1989) has recently presented an overview of solar and stellar flares. These transient phenomena fit in a general framework that is described by a rapid (~seconds) initial outburst followed by a more gradual decay. The physical mechanism that leads to flares is unknown but is believed to involve magnetic reconnection. We present optical observations of a giant stellar flare ( $\Delta U = 5$

mag) at high spectral and temporal resolutions, in both the blue and red spectrum. It is hoped that they will give insight on the response of the chromosphere to the flare energy, and the physical mechanisms which transport the energy.

## 2. OBSERVATIONS

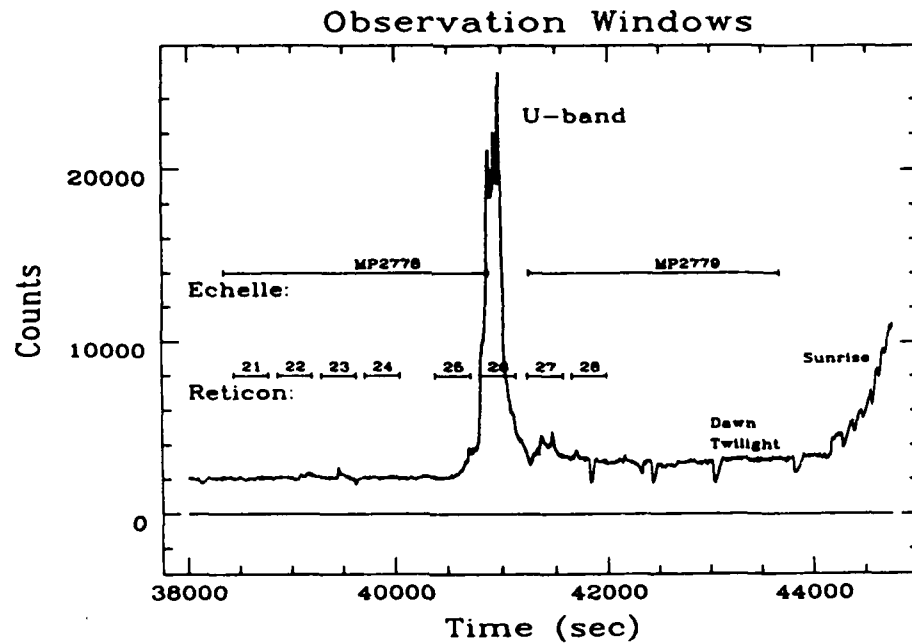
Three telescopes were employed in simultaneous observations of the dMe 5.6e flare star UV Ceti on the night of 8 September 1979 (UT). These telescopes were the 4-m Mayall at Kitt Peak National Observatory (KPNO) with the echelle spectrograph; the 2.1 m at Steward Observatory with the Reticon spectrograph; and the 0.9 m at KPNO with the three-channel photometer and *UBV* filters. The *IUE* satellite observed the star on the following day obtaining a single spectrum (Linsky *et al.* 1982). Both stars of the UV Ceti binary system were in the apertures of all telescopes. The seeing on Kitt Peak was  $\sim 2$  arcsec.

At 1115:35 (UT) on 8 September, UV Ceti began to brighten slowly. All three ground based telescopes were observing the star at this time. Shortly thereafter, the star erupted dramatically at 1119:55 (UT). Unfortunately, the 4-m Mayall telescope had ceased observing for about  $\sim 6^m$  to change plates. By the time it was observing again, the flare was already rapidly declining. We indicate in Fig. 1 the observing durations of each echelle plate and each Reticon scan superimposed upon the photometric light curve of the flare in order to illustrate the physical events observed by each instrument. Dawn terminated observing well before the star had completely returned to its quiescent state.

### 2.1 Echelle Spectrograph: Red Spectra

Four data plates and one spot-calibration plate were taken of UV Ceti with the 4-m Mayall telescope at KPNO. Unfortunately, no spectral- or flux-calibration plates were made. The data plates were exposed with the same instrument configuration on IIIaJ emulsion at a dispersion of  $2.88 \text{ Å mm}^{-1}$ . The spectral resolution was  $0.16 \text{ Å}$  at H $\alpha$ , and the spectral range was 5200–7000 Å. They were time trailed by shifting the plate in cross dispersion with  $35 \mu\text{m}$  steps, corresponding to one-fourth arcsec on the sky. Thus, each step moved the spectrum only one-eighth of the seeing disk, thus producing a smooth cross-dispersion trail. The stepping rate was slaved to the brightness of the star by diverting a small fraction of the beam into a photometer. The combination of step size, stepping rate, and seeing disk yielded a temporal resolution of  $\sim 6^m$ . The start-stop times and the exposure lengths of each plate are listed in Table 1.

The plates were digitized on a PDS microdensitometer at the High Altitude Observatory of the National Center for Atmospheric Research. A  $16 \times 40 \mu\text{m}$  aperture was used corresponding to  $0.051 \text{ Å} \times 1.3 \text{ min}$ . The chemical plate fog was measured on each plate and subtracted. Spot densities were measured and fit with a cubic spline to tabulated intensities provided by KPNO. The spline was applied to each plate to transform the density of each pixel to



### UV Ceti (8 Sept 79)

FIG. 1. Echelle-plate and Reticon-scan observing windows superimposed on the photometric light curve.

relative intensity. Measurements between each echelle order were made of the image-tube illumination and subtracted.

Time trailing the plates left no room for a wavelength calibration spectrum. However, three spectral lines, He  $\lambda$ 5876, and Na  $\lambda$ 5890, 5896, were present on a single echelle order. These were used to determine the spectral dispersion at that plate position,  $2.875 \text{ \AA mm}^{-1}$ . This datum was used to register a print (provided by KPNO) of a wavelength calibration spectrum taken with the same instrument configuration which provided calibration of the entire plate.

It was difficult to derive stepping times for the spectra. But the spectra included the night sky line due to O  $\lambda$ 5577. Assuming its intensity was constant during a 45 min exposure, the changes in the measured line-flux will give the stepping rate. Within the measurement errors ( $\sim 10\%$ – $15\%$ ), the line flux and thus the stepping rate was found to be constant.

TABLE 1. Echelle plate information.

Plate ID	Starting Time (UT)	Stop Time (UT)	Exposure (min)
MP2776	0839.5	0927.4	47.9
MP2777	0937.0	1033.0	56.0
MP2778	1039.1	1121.3	42.2
MP2779	1127.5	1207.8	40.3

### 2.2 Reticon Spectrograph: Blue Spectra

Twenty-eight digital spectra were recorded with the 2.1-m telescope at Steward Observatory. The spectral range was 3500–4600  $\text{\AA}$ , and the spectral resolution was 3.8  $\text{\AA}$ . All exposure times were  $5^m 35^s$ . We list in Table 2 the start times of each spectrum. The flare slow-rise began during scan no. 25, after which three more scans were taken: one each of the major impulsive phase, a subsequent minor impulse, and the relaxation phase.

The Reticon data were reduced and calibrated with standard procedures utilizing simultaneous sky measurements in a second aperture, wavelength calibration scans, quartz scans, and standard star measurements. All emission line flux measurements are given in terms of total line flux above the local continuum.

### 2.3 Photometer: *UBV*

UV Ceti was continuously monitored with the three-channel photometer on the 0.9-m telescope at KPNO. This instrument simultaneously recorded the output from three photometers each with its own filter. The Johnson system of *UBV* filters was employed with a  $5^s$  integration time. Sky measurements were made approximately every  $10^m$  for  $1^m$  duration. No standard star or extinction measurements were made.

The data were reduced first by fitting and subtracting a curve to the sky measurements. We adopted standard cosecant-law coefficients to correct for atmospheric extinction. They were flux-calibrated by comparing the quiescent

TABLE 2. Reticon scan information.

Scan #	Start (UT)	Scan #	Start (UT)
1	0803:03	15	0954:16
2	0811:32	16	1001:14
3	0824:47	17	1012:49
4	0832:04	18	1019:55
5	0839:24	19	1026:53
6	0846:28	20	1033:51
7	0853:36	21	1040:49
8	0900:35	22	1047:51
9	0907:43	23	1054:55
10	0919:30	24	1101:53
11	0926:31	25	1113:05
12	0933:25	26	1120:01
13	0940:19	27	1127:21
14	0947:17	28	1134:13

Note to TABLE 2

All single scan integration times are  $5^m35^s$ .

fluxes to published values. Table 3 summarizes the parameters used.

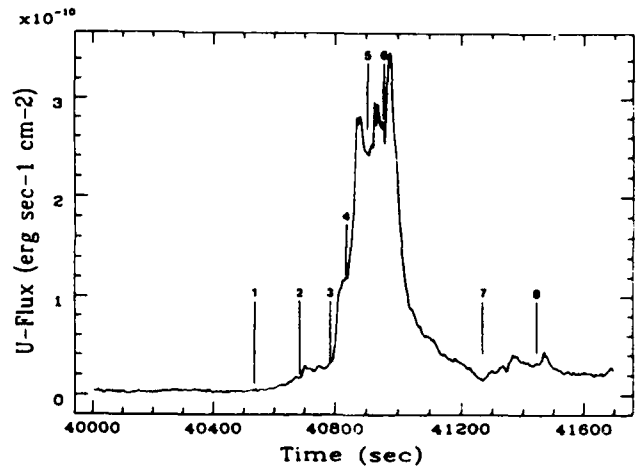
### 3. ANALYSIS AND DISCUSSION

#### 3.1 Photometry

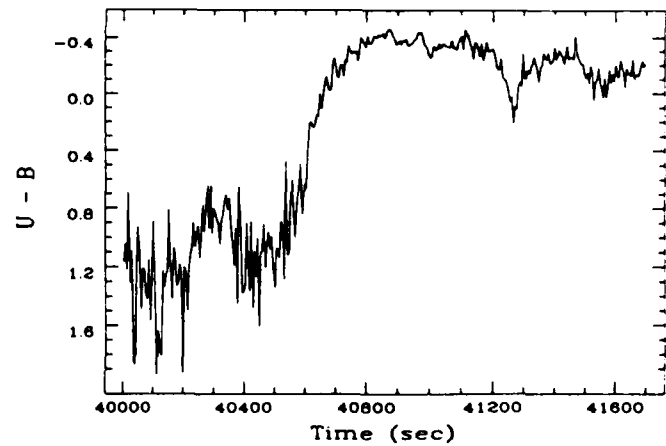
We identify eight events in the expanded view of the light curve as indicated in Fig. 2(a). Figures 2(a)–2(c) are

TABLE 3. Photometry reduction parameters.

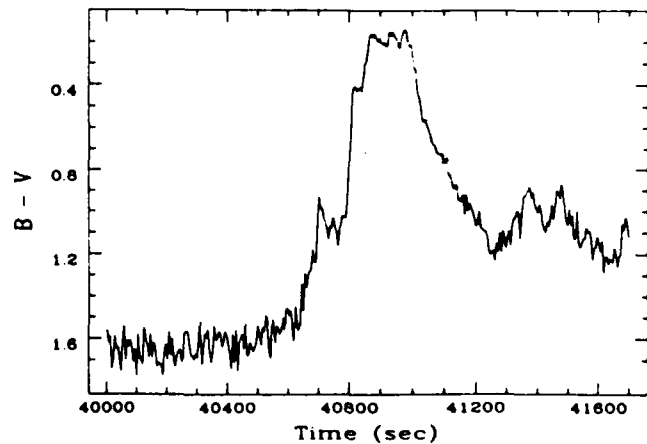
Filter	Extinction Coef.	Quiescent Count	Relative Magnitude
U	0.56	543	14.86
B	0.26	1900	13.66
V	0.17	6796	12.01



(a) UV Ceti



(b) UV Ceti



(c) UV Ceti

FIG. 2. (a) Photometric U band, (b)  $U-B$  light curve, and (c)  $B-V$  light curve. We identify 8 flarelike events in the U-band light curve.

the photometric U-band flux, and ( $U-B$ ) and ( $B-V$ ) colors, respectively. All three colors respond slowly to the two slow events, rapidly to the six impulsive events, and slowly return to quiescence. Table 4 lists the start times, rise times, flux enhancement ( $\text{erg s}^{-1} \text{cm}^{-2} \text{\AA}^{-1}$ ; hence-

TABLE 4. Photometric event times.

Event #	Time (UT)	Rise time	$\delta$ Flux (U)	$\delta F/F_q$
1	1115:35	270 <sup>s</sup>	37.5	12.3
2	1118:10	15 <sup>s</sup>	10.7	3.5
3	1119:55	20 <sup>s</sup>	73.2	24.0
4	1120:45	30 <sup>s</sup>	134.0	44.0
5	1121:55	20 <sup>s</sup>	44.8	14.7
6	1122:45	15 <sup>s</sup>	78.7	25.8
7	1127:50	100 <sup>s</sup>	22.3	7.3
8	1130:55	15 <sup>s</sup>	8.5	2.8

Notes to TABLE 4

Fluxes are in units of  $10^{-12}$  erg  $s^{-1}$   $cm^2$ .  
The observed  $U$ -band quiescent flux is  $F_q = 1.77 \pm 0.32$  in these units.

forth abbreviated cgs) above the level from which the event began, and the enhancement relative to quiescence ( $F_q$ ). Events 1 and 7 were slow with rise times of several minutes, while the others were impulsive with rise times of fractions of a minute. Events 3, 4, 5, and 6 are closely clustered and together constitute the major outburst. The decline from this series of impulses exhibits two phases: the initial rapid decline which lasts 60 s during which the flare flux declines by 50%, and the subsequent slow phase which never attains quiescence in the four minutes before event 7 begins. The last two events (7 and 8) may be unrelated to the first six events. As discussed in Sec. 1 the complexity of the flare light curve suggests a complicated flare morphology, i.e., different regions of the flare may be "going off" at different times and decaying at different rates.

None of the color indices, ( $U-B$ ), ( $B-V$ ), or ( $U-V$ ), are useful probes into resolving the fraction of light-enhancement arising from the continuum and that from emission lines. Ideally, one of the colors would be solely affected by the flare continuum and another solely by emission lines. This is not the case for any of these three colors. The  $U$ -band is dominated by the flare continuum which peaks in the violet (see below); however, it also is significantly affected by the Balmer series including  $H\epsilon$  and  $H\zeta$ , as well as  $Ca II H$  and  $K$ . The  $B$  band is dominated by chromospheric emission lines, but the flare continuum is also strong in the blue during the peak of the major impulses. The  $V$  band is affected by  $H\alpha$  enhancement and the appearance during the flare of the helium and sodium lines along with a host of faint iron lines. The flare continuum is determined with the Reticon to be strong and slowly falling out to 4600 Å ( $\sim 10^{-13}$  cgs), only 300 Å from the blue edge of the  $V$  band at 4900 Å. It is uncertain how much flare continuum the  $V$  band observed but it is likely to be

significant. Thus, no color index is very good for resolving the contribution of the continuum from the emission lines.

We estimate the total radiative flare energy in the  $U$  band by integration of the observed flux with respect to the preflare quiescent level combined with a duration of 700 s. This procedure yields a total flare energy in the  $U$  band of  $5 \times 10^{31}$  ergs. The total flare energy in white light can be inferred from the scaling relation between white-light flare luminosity ( $L_w$ ) and the flare luminosity in the  $U$  band ( $L_U$ ), or  $L_w \approx 2.4L_U$  as given by Lacy *et al.* (1976). We thus find a total white-light flare energy of  $2.0 \times 10^{32}$  ergs. These values invite a comparison of the flare luminosity in white light to the total stellar bolometric luminosity. Adopting  $\log L_{bol} = 30.74$  for UV Ceti (Bookbinder 1985) and the aforementioned estimate of the white-light flare luminosity yields  $L_w/L_{bol} \approx 3.1 \times 10^{-2}$ , or  $\sim 3\%$  of the stellar bolometric luminosity. By contrast, the coronal and chromospheric heating efficiencies, as represented by the ratio of the relevant band or line luminosities to the bolometric luminosity, are each of the order of  $10^{-3}$  for UV Ceti (Bookbinder 1985; Linsky *et al.* 1982). Hence, the flare heating mechanism proceeds at an efficiency which is significantly enhanced compared to chromospheric and coronal heating processes.

### 3.2 Continuum Emission

The violet continuum began rising during the first two events and dramatically rose, even out to 4600 Å, with the four following impulses [Figs. 3(a)–3(e)]. No continuum enhancement was observed by the echelle at 5577 Å; however this instrument missed the dramatic continuum flash of the impulsive phase.

Thermal bremsstrahlung from a homogeneous, plane-parallel slab of gas of depth  $D$ , density  $n_e$ , and temperature  $T_e$  was compared to the observed flare continuum radiation. For purposes of calculation of the source function, the slab was considered to be infinitely wide, though for calculation of the total flux it was given a width  $W$  and area  $A = W^2$ . Three temperatures were chosen: the flux for  $T_e = 13\,000$  K will peak at 3700 Å, as observed, when optically thick (blackbody radiation); the flux for  $T_e = 36\,000$  K will decrease rapidly blueward of 3700 Å when optically thin; and  $T_e = 5 \times 10^5$  K was investigated to see if a superheated chromosphere could reproduce the observations before dynamical expansion lowered the density. Each temperature was tested at three optical depths:  $\tau = 0.1, 1.0, 10$ , and the intensity was evaluated normal to the surface. The intensity  $I_\nu$  is

$$I_\nu(n_e, T_e, D) = S_\nu(1 - e^{-\alpha_\nu D}). \quad (1)$$

The frequency-dependent source function  $S_\nu$  is given by

$$S_\nu(n_e, T_e) = \frac{\epsilon_\nu}{\alpha_\nu}, \quad (2)$$

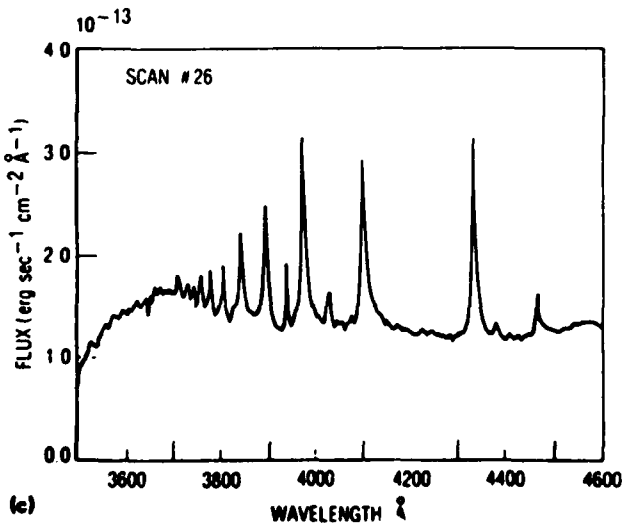
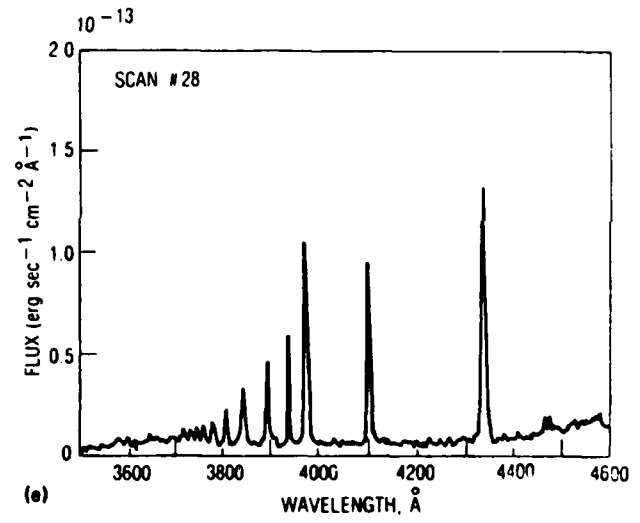
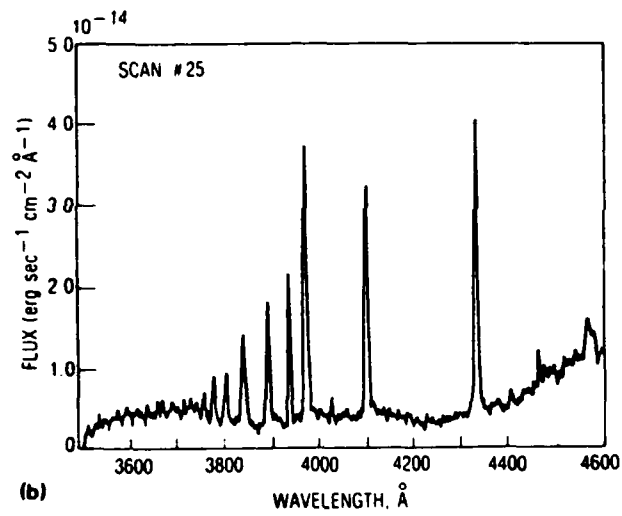
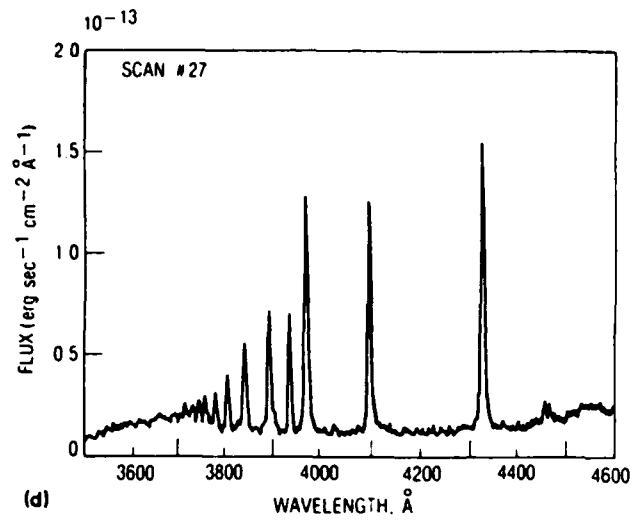
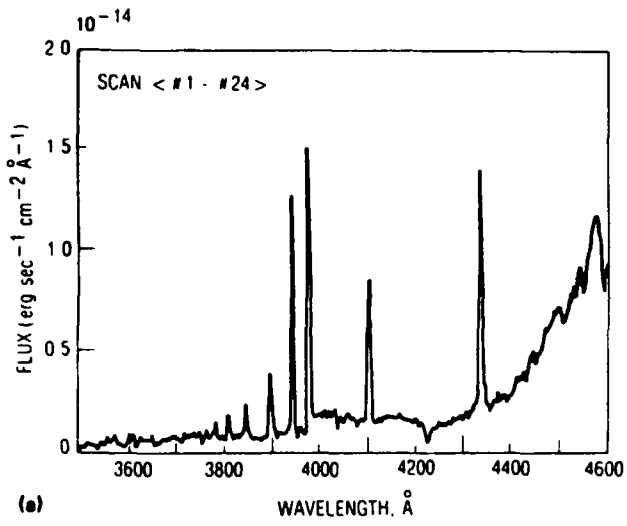


FIG. 3. (a)-(e) Time sequence of the final five Reticon spectra. Note varying vertical axis scales, particularly for the average of scans 1-24 (top).

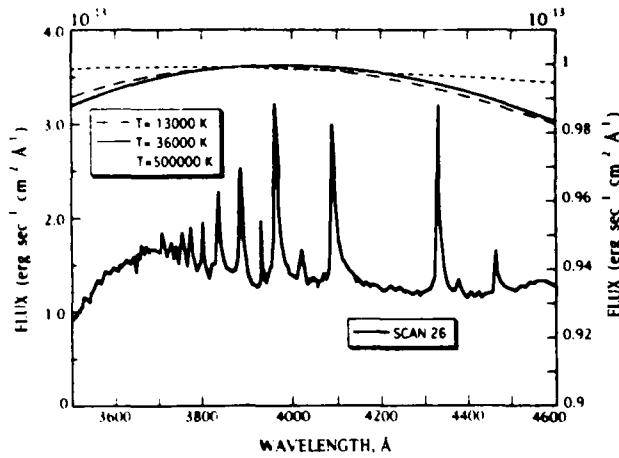


FIG. 4. Synthesized thermal bremsstrahlung spectra and the observed spectrum in the blue at flare maximum. The computed peak spectral flux is forced to  $f_{\lambda} = 10^{-13} \text{ erg s}^{-1} \text{ cm}^{-2} \text{ \AA}^{-1}$ . The vertical scale on the right applies to the calculated spectra. The ordinate on the left is the observed monochromatic flux of the flare spectrum. The bremsstrahlung spectra are calculated for electron temperatures of 13 000, 36 000, and  $5 \times 10^5$  K, respectively.

where

$$\epsilon_v = 6.8 \times 10^{-38} T_e^{-1/2} n_e^2 \times \exp\left(-\frac{h\nu}{kT_e}\right) \bar{g}_{ff} \text{ erg s}^{-1} \text{ cm}^{-3} \text{ Hz}^{-1} \quad (3)$$

and

$$\alpha_v = 3.7 \times 10^8 T_e^{-3/2} n_e^2 \bar{g}_{ff} \text{ cm}^{-1}. \quad (4)$$

In these expressions,  $\epsilon_v$  is the emissivity,  $\alpha_v$  is the opacity,  $\bar{g}_{ff}$  is the Gaunt factor averaged over a Maxwellian distribution, and all other symbols represent standard physical quantities (Rybicki & Lightman 1979). The surface area of the emitting region is given by  $A = 4d^2 f_{\lambda} / I_{\lambda}$ , where  $f_{\lambda}$  is defined by the monochromatic flux received at the earth at 3700 Å ( $\sim 10^{-13}$  cgs) and we adopt a distance to UV Ceti of  $d = 3.75$  pc (quoted by Linsky *et al.* 1982).

The fits for each temperature, none of which is satisfactory, are displayed in Fig. 4, overplotted on the Reticon scan recorded during maximum flare emission. The two best fits are optically thick emission at  $T_e = 13$  000 K, and marginally thick emission at  $T_e = 36$  000 K, but both fail to reproduce the rapid flux falloff blueward of 3600 Å. For optically thin emission,  $A \sim n_e^{-2}$ , while for optically thick emission  $A$  is not a function of electron density. The apparent UV cutoff shown in the data must be treated with caution, however. These observations were obtained through relatively large and changing air masses. As such, the calibrations at these short wavelengths are only approximate.<sup>3</sup> The Balmer jump is both small ( $\sim 7\%$  of the continuum flux) and *in absorption*. Many models (cf Cram

& Woods 1982) produce Balmer continuum in emission contrary to these observations.

### 3.3 Line Emission: Echelle Spectra

There are four visible emission lines in the quiescent spectra: H $\alpha$ , Na I  $\lambda\lambda 5890, 5896$  (both very weak), and O I  $\lambda 5577$  (night sky line). When the flare erupts, H $\alpha$  and the Na D lines strengthen considerably, and He I  $\lambda 5876$  and He I  $\lambda 6678$  each appear along with a host of faint lines that are probably Fe I and Fe II features between 5200–5400 Å. Furthermore, strong and broad H $\alpha$  wings appear which remain until the termination of observations.

Relative fluxes ( $F_{\lambda}$ ) and equivalent widths ( $W_{\lambda}$ ) were measured for each line at several times (Table 5). As no calibrated red spectrum of UV Ceti could be found, the absolute line fluxes could not be derived from the equivalent widths. The relative fluxes of a given spectral line at different times can be compared, however fluxes of different lines cannot be intercompared. Equivalent widths of different lines can be intercompared. The advantage of the relative fluxes is that the errors are much smaller. The echelle plates were exposed to maximize the S/N ratio of H $\alpha$  without saturating it. Unfortunately, this caused the continuum to be underexposed resulting in poor S/N for the continuum level. Thus, while the line flux values obtained for the well exposed emission line are relatively accurate, the equivalent widths for the same lines are much poorer due to continuum level uncertainty.

It is difficult to accurately disentangle the H $\alpha$  emission profile from a changing continuum profile (including absorption lines from non-flare regions of the star and molecular line features). Complicating the H $\alpha$  profile is a decline in the continuum intensity somewhere within the line. Closer inspection shows that, even well away from the line center, the continuum is 25% lower on the red side of the line than on the blue side. The cause is probably a molecular absorption band, but no plausible transition could be identified in either Kopp *et al.* (1974) or Pease & Gaydon (1976). Lacking further information, the H $\alpha$  continuum was simply chosen to be the mean of the blue-wing and red-wing continua.

Important parameters characterizing key emission lines that appear in the echelle spectra were deduced through Gaussian fits to each line profile. The results are given in Table 5 where the line profile is defined by choosing a continuum, a Doppler width, a peak flux, and a line centroid. Examples of these fits are displayed in Fig. 5 for features in outburst. The Na I D lines ( $\lambda\lambda 5890, 5896$ ) and the He I triplet ( $\lambda 5876$ ) and singlet ( $\lambda 6678$ ) lines proved to be Gaussian in shape indicating that there is no pressure broadening and that they are optically thin. The H $\alpha$  line in quiescence is shown in Fig. 6. Gaussian profiles were found to fit the quiescent H $\alpha$  line core, but not the line center which includes a central reversal and which is optically thick. The occurrence of the central reversal is a non-LTE effect arising in optically thick chromospheric emission lines, as is often observed in the H $\alpha$  emission lines in dMe stars (Worden *et al.* 1981). Interestingly, an H $\alpha$  profile

<sup>3</sup>Observations of other flares are needed to confirm the reality of this ultraviolet fall off. More recent spectrophotometric stellar flare observations in this wavelength regime do not exhibit this behavior. The most likely cause in these data is atmospheric extinction.

TABLE 5. Line profile analysis.

Time (UT)	$F_\lambda$ (rel.)	% Error	$W_\lambda$ (Å)	$\Delta\lambda_D$ (Å)
<b>H<math>\alpha</math></b>				
1046	1.22	12	7.72	0.9
1108	1.66	9	10.6	0.9
1127	6.50	5	67.5	0.9
1148	4.80	5	51.1	0.9
1208	3.27	7	33.8	0.9
<b>He I <math>\lambda</math>5876</b>				
1127	0.470	8	15.5	0.54
1148	0.308	10	7.85	0.54
1208	0.213	19	4.39	0.56
<b>He I <math>\lambda</math>6678</b>				
1127	0.108	60	4.07	0.54
1148	0.076	60	2.69	0.54
1208	0.035	50	1.03	0.54
<b>O I <math>\lambda</math>5577</b> (night sky)				
1127	0.069	22	1.60	0.16
1148	0.085	13	2.38	0.16
1208	0.065	23	1.92	0.16
<b>Na D <math>\lambda</math>5890</b>				
1127	0.0526	8	3.81	0.55
1148	0.0460	9	2.59	0.55
1208	0.0386	16	2.11	0.55
<b>Na D <math>\lambda</math>5896</b>				
1127	0.0341	9	2.08	0.55
1148	0.0291	16	1.49	0.55
1208	0.0256	11	1.46	0.55

NOTE TO TABLE 5

relative fluxes for a given line may be compared at different times, but may not be intercompared between lines. Equivalent widths may be intercompared but the errors are worse.

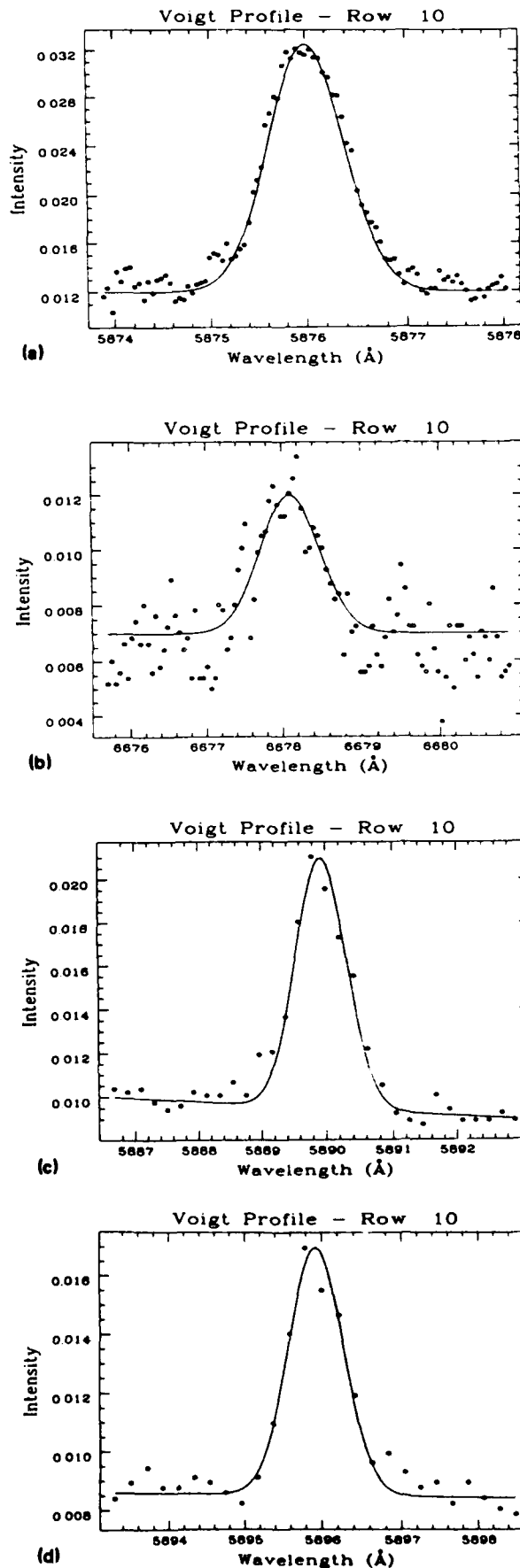


FIG. 5. Observed echelle line profiles in outburst with synthesized Gaussian profiles superimposed. The features include (a) He I  $\lambda$ 5876, (b) He I  $\lambda$ 6678, (c) Na I  $\lambda$ 5890, and (d) Na I  $\lambda$ 5896. The line profiles were recorded on echelle plate MP2779.

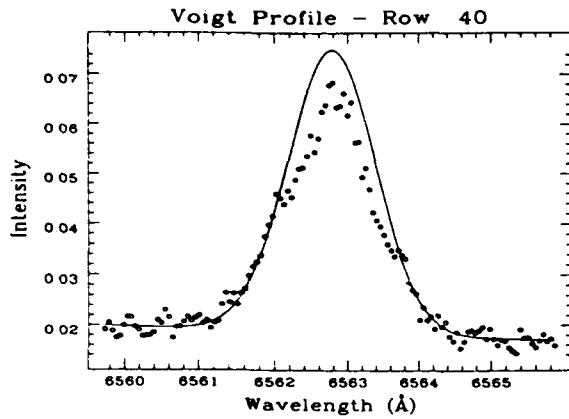


FIG. 6. The H $\alpha$  line profile in quiescence recorded on echelle plate MP2778. Note the appearance of a small but discernible central reversal. See the text for a discussion.

during outburst, as seen in Fig. 7(a), exhibits evidence of a central reversal. We note that this can indicate the absence of a high pressure transition region at the site of the H $\alpha$  flare emission, at least subsequent to flare maximum (Balunas *et al.* 1979). For H $\alpha$  during outburst, a Doppler profile was found to fit the core, which is saturated, but could not fit the core and wings simultaneously. The

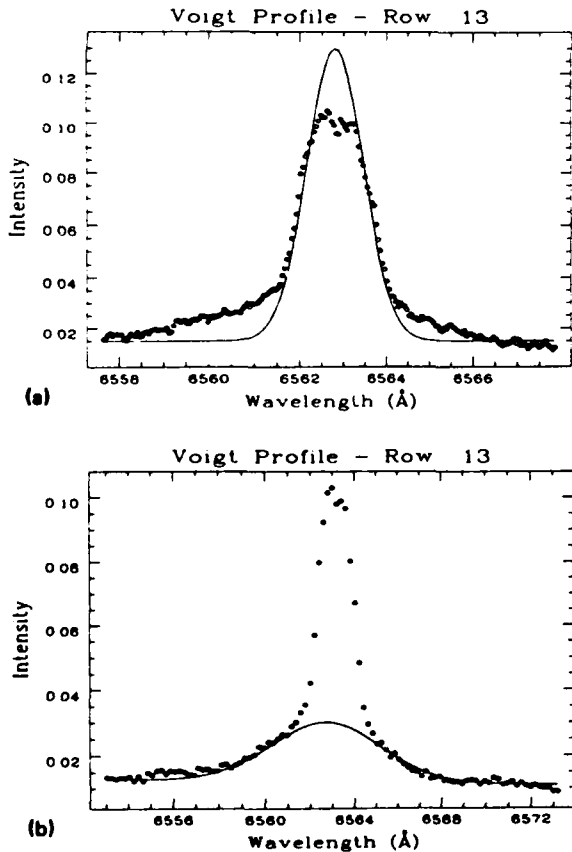


FIG. 7. Observed H $\alpha$  profile in outburst with synthesized Gaussian profile of line core (a) and wings (b) superimposed. A central reversal is present in the line core. Note that for purposes of clarity, the scales of the ordinate and abscissa, and the number of points plotted, differ between (a) and (b) though the profile is the same.

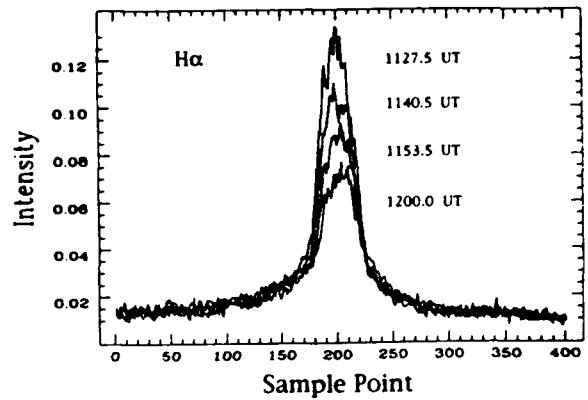
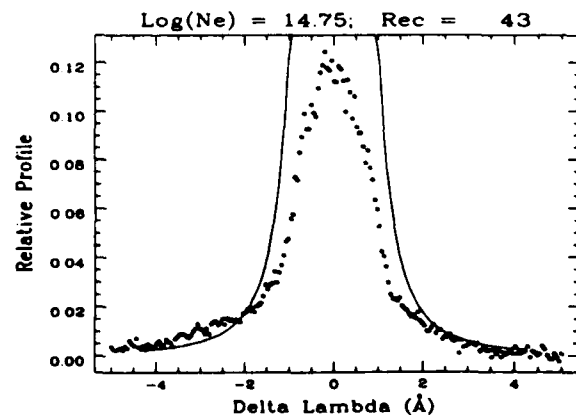


FIG. 8. Time sequence of observed H $\alpha$  profiles following maximum light.

wings could, however, be fit by a blueshifted ( $\Delta\lambda_{bs} = -1.5 \text{ \AA}$ , or  $69 \text{ km s}^{-1}$ ), highly broadened ( $\Delta\lambda_D = 3.5 \text{ \AA}$ ), low-peak-flux Doppler profile [Fig. 7(b)]. We interpret this as rising (evaporating) chromospheric material with either a thermal temperature,  $T_e \sim 10^6 \text{ K}$ , or a microturbulent velocity,  $v_{turb} \sim 150 \text{ km s}^{-1}$ , or a combination involving a lower temperature and velocity. We note that a temperature  $\sim 10^6 \text{ K}$  would lead to complete hydrogen ionization. Clearly, the observed flare line widths are not dominated purely by thermal broadening. Chromospheric material continues to rise for more than 40 min after the impulsive phase of the flare. During this time, the wing blueshift and width do not vary to within an error of  $0.5 \text{ \AA}$ , respectively. An illustration of the temporal evolution of the flare H $\alpha$  emission line profile is given in Fig. 8.

A Stark profile (Underhill & Waddell 1959) was fit to H $\alpha$  during outburst. Because the Stark profile away from the line center is a power law ( $\lambda^{-5/2}$ ), and the observed line is uncalibrated allowing arbitrary intensity scaling, the profile fit is independent of electron density. Figure 9 is a Stark profile compared to H $\alpha$  at maximum brightness. The difference in red and blue continua is clearly visible. The profile satisfactorily fits one wing but begins to deviate significantly within  $\Delta\lambda = 2 \text{ \AA}$ . This asymmetry, and the fact that calculations made by Phillips *et al.* (1988) for



H-alpha Stark Broadening  
FIG. 9. Synthesized Stark profile superimposed on H $\alpha$  as seen shortly after maximum light.

another flare on UV Ceti show that Stark broadening is not significant until electron densities exceed  $10^{13} \text{ cm}^{-3}$ , points to line broadening mechanisms other than Stark or thermal broadening. We conclude (as did Phillips *et al.*) that directed mass outflows, similar to those seen in solar flares, with outflow velocities in the range of  $\sim 100 \text{ km s}^{-1}$ , best explain the observed profile where the line is probably still optically thin. This casts some doubt upon Stark broadening as the principal physical mechanism producing the line wings. Byrne (1989) also discusses evidence for significant mass motions in stellar flares.

These echelle observations suggest that the site of H $\alpha$  flare emission is characterized by densities  $n_e < 10^{13} \text{ cm}^{-3}$  and upward moving material. Therefore, the likely origin of the strong enhancement in the line emission during the flare is the filling of a large flare volume with plasma at chromosphericlike densities. This interpretation of the results of our time-resolved optical spectroscopy is consistent with prior inferences, based on x-ray observations of flares on dMe stars, of large flare volumes with radii of 0.1–0.2  $R_*$  (Kahn *et al.* 1979; see also Haisch *et al.* 1981). Furthermore, Worden *et al.* (1979) reported, using the same kind of time-resolved echelle spectroscopy as in this investigation, that line broadening in H $\alpha$  and H $\beta$  was not observed in stellar flares, although the line center intensity increased by over a factor of 2 during some of the flares they recorded. Again, this behavior is consistent with an increase in emission measure that is due mainly to an increase in the emitting volume of hot plasma during a large stellar flare (see also Schneeberger *et al.* 1979).

### 3.4 Line Emission: Reticon Spectra

We list in Table 6 all the lines visible in the blue spectra with measured fluxes as a function of time. The Ca II H and K lines are strong, and the Balmer series is evident out to H14, even during quiescence. Some flare emission lines that are either unknown or only tentatively identified are given in Table 7. Haisch & Giampapa (1985) also observed unidentified lines in a flare on YZ CMi, albeit at different wavelengths. They attributed these features to optically thin emission in neutral metal species excited by the flarelike enhancement of the Ca II resonance lines.

All Balmer emission lines rose more than a factor of 2 with the low level onset of the flare (Fig. 10). During the full outburst they rose an order of magnitude on a time-scale of  $\sim 5^{\text{m}}$ . By events 7 and 8, they had fallen a factor of 2, and another factor of 2 by scan no. 28. The lower lines, H $\gamma$  and H $\delta$ , approach equal flux during maximum outburst indicating that these lines are optically thick. Given the fast rise and fall observed in the photometry, observations at higher temporal resolution may well show much higher flux increases and a strong Balmer increment. The flux of He was derived by assuming a Ca II resonance line ratio, H/K  $\approx 1.1$  (Giampapa *et al.* 1982b). The resulting flux appears reasonable when compared with the other Balmer lines. After maximum light the line ratios gradually return to quiescent values.

The Ca II H and K line fluxes initially fall a factor of 3

TABLE 6. Reticon emission line fluxes.

Line	Quiescence	Scan #25	Scan #26	Scan #27	Scan #28
Mg II $\lambda 4481$	-	13.5	50.5	42.8	40.0
He I $\lambda 4471$	-	27.3	234.0	81.0	46.7
He I $\lambda 4387$	1.88	19.1	86.1	27.3	
H $\gamma$	103.0	268.0	2770.0	1520.0	1130.0
H $\delta$	47.3	193.0	2650.0	1080.0	696.0
?	-	5.37	67.0	10.7	13.1
He I $\lambda 4025$	2.18	8.67	241.0	46.5	26.4
He+Ca II H	132.0	195.0	2070.0	1100.0	66.0
He (estimate)	26.4	153.0	1790.0	768.0	404.0
Ca II K	96.0	38.6	257.0	302.0	237.0
H $_8$	18.9	111.0	1280.0	555.0	270.0
H $_9$	9.5	97.4	950.0	388.0	237.0
H $_{10}$	7.7	39.2	354.0	215.0	115.0
H $_{11}$	5.3	29.7	291.0	108.0	71.5
H $_{12}$	2.2	14.8	188.0	84.2	42.3
H $_{13}$	1.5	3.6	81.2	58.5	40.0
H $_{14}$	1.2	2.9	75.0	32.0	21.6
?	1.4	9.0	127.0	38.5	30.8

Note to TABLE 6

Observed fluxes in units of  $10^{-15} \text{ erg s}^{-1} \text{ cm}^{-2}$ .

before rising above quiescent values. The fall of the H line, which is blended with the rising He, is implied by the flux constancy of the blend. Following the decline, Ca II K rises only about a factor of 2 above quiescence and remains there. Possible causes are evaporation of the lower chromosphere (cf. Antonucci & Donner 1983), diminishing of the source function by a shock wave (Livshits & Badalyan 1981), or ionization of Ca $^+$  to Ca $^{++}$  by x rays.

The fall of the calcium emission may have the potential

TABLE 7. Unidentified Reticon emission lines.

$\lambda_{\text{obs}}$ (Å)	Remarks
3702	Unknown
3788	Blended with H $_{10}$
3811	Unknown weak feature
3820	Possibly He I $\lambda 3819$
3856	Possibly He I $\lambda 3856$ or Si II $\lambda 3856$
3862	Possibly Si II $\lambda 3862$
3873	Blended with H $_8$
4075	Unknown weak feature

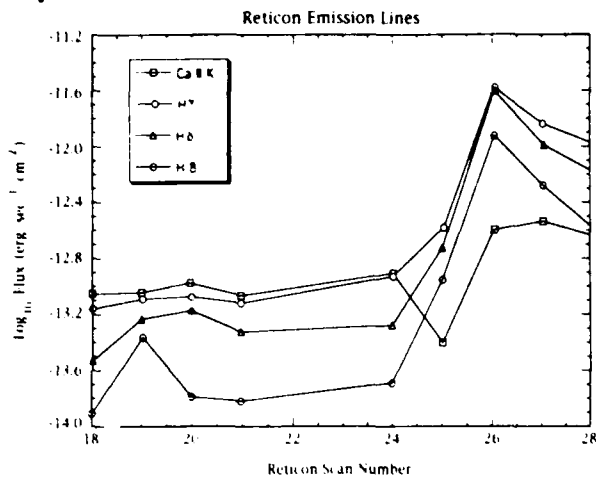


FIG. 10. Balmer line time series of the observed total line flux as recorded with Reticon. The behavior of the total flux in the Ca II K line is also shown.

of qualitatively determining the fraction of the stellar surface covered with chromospheric emission. To do this, the photospheric source function must be known, for though 60% of the *net* line emission has been removed, after correcting for an unknown effect upon the line flux by photospheric absorption, perhaps substantially less than 60% of the *gross* chromospheric emission has disappeared during the impulsive phase. For the sake of illustration assume there is no photospheric absorption or emission. If chromospheric calcium emission is uniformly spread over the stellar surface, then whatever affected the calcium lines must have affected 60% of the observable stellar surface, which seems implausible. However, the chromospheric emission may be strongly concentrated about a few star-spot groups. Such a large flare as we observed probably came from the largest and therefore the most chromospherically emissive region on the visible surface of the star. A flare of this magnitude then could plausibly disturb the calcium source function and significantly reduce the line emission. Arguments of this kind become less relevant if photospheric absorption significantly affects the line flux. Thus, detailed knowledge of the photospheric calcium source function is important to the interpretation of this phenomenon.

The behavior of the Ca II H and K lines is, at any rate, a topic for future study. The YZ CMi flare observed by Haisch & Giampapa (1985) also exhibited anomalies in these lines. In those observations, the Ca II K line strengthened relative to the H line. The latter may actually have decreased during the flare. One additional mechanism, apart from those mentioned above, is the *disparition brusque* phenomenon of a classic solar two-ribbon flare (Giampapa *et al.* 1982a). Haisch *et al.* (1983) used this model to describe their observations of a flare on Proxima Centauri (dM5.5e). In a solar two-ribbon flare, early stages of the event are often characterized by the ejection (*disparition brusques*) of quiescent prominences. The passage of this cool material in front of the flaring region can

produce line and continuous absorption, depending on the geometry and physical conditions within the absorbing material. This could explain the Ca II H and K anomalies observed in the early stages of the event on UV Ceti described in this work.

The applicability of a two-ribbon flare model to the flare described herein can be briefly examined from a purely energetics perspective. In particular, the power of a two-ribbon flare scaled to appropriate stellar parameters is given by (Giampapa 1986)

$$P = 5 \times 10^{34} V_{100} B_0 R_*^2 (L/R_*)^6 (l/R_*)^{-4} \text{ ergs s}^{-1},$$

where  $V_{100}$  is the velocity of mass motions in units of 100 km s<sup>-1</sup>,  $B_0$  is the surface magnetic field strength in kG in the active region,  $R_*$  is the stellar radius in solar radii,  $L$  is the characteristic size of the active region, and  $l$  is the size of the filament. The value of  $B_0$  is not known for UV Ceti. However, following the direct measurement of surface magnetic field strength and filling factor by Saar & Linsky (1985) for the dMe flare star AD Leo, we adopt  $B_0 \sim 4$  kG for UV Ceti. In addition, we assume that the scale of the active region filament is of the same order as that of the active region itself, i.e.,  $l \sim L$ . Then using  $V_{100} \approx 0.7$  as inferred from our observations, and a stellar radius of  $R_* = 0.22 R_\odot$ , we find for the cases of a compact ( $L \sim 0.1 R_*$ ) and an extensive ( $L \sim R_*$ ) active region on the stellar surface that  $P \sim 10^{32}$  ergs s<sup>-1</sup> and  $P \sim 10^{34}$  ergs s<sup>-1</sup>, respectively. Thus, the energetics of this major flare event on UV Ceti appear to be easily satisfied by that of a two-ribbon flare model. Whether in fact two-ribbon flares occur on dMe flare stars is, however, unknown.

#### 4. SUMMARY

We have presented simultaneous optical observations of a  $\Delta U = 5$  mag flare on UV Ceti obtained with the 4-m Mayall echelle spectrograph (5200–7000 Å), 2.1-m Steward Observatory Reticon (3500–4600 Å), and the 0.9-m KPNO three-channel (*UBV*) photometer on 8 September 1979. These observations give both high temporal and spectral resolution of the complex sequence of flare events. The impulsive phase is dominated by a strong violet continuum which rises and fades in 4<sup>m</sup>. Thermal bremsstrahlung spectra were synthesized but none satisfactorily represented the data.

Balmer emission, resolvable out to H14 and enhanced by up to a factor of 20, remained above quiescence beyond 40 min after outburst. The flux of Hγ and Hδ were nearly equal at maximum light, and the latter would probably be brighter with higher time resolution. Ca II H and K initially fell a factor of 3 before rising above its preflare level thus indicating a significant and rapid change in the lower chromosphere. To interpret this phenomenon the photospheric Ca II source function must be known so that the impact upon the gross chromospheric emission may be derived. In addition, three neutral helium lines, λ4025, λ4387, and λ4471, strengthened or appeared in the blue spectrum.

High spectral resolution Doppler profiles were fit to the emission lines observed with the echelle, namely,  $H\alpha$ ,  $\text{Na I } \lambda\lambda 5890, 5896$ , and  $\text{He I } \lambda\lambda 5876, \lambda 6678$ . All lines were well fit except  $H\alpha$  which is clearly saturated. One  $H\alpha$  flare profile exhibits a small central reversal (as does the quiescent profile) which is a characteristic of the non-LTE formation of an optically thick emission line. The Doppler widths of none of the lines changed during the flare. However, strong  $H\alpha$  wings appeared after the impulsive phase which persisted until the end of the observations 40 min later. Stark broadening was investigated as a source of the wings. Though it cannot be conclusively ruled out, it is in doubt because it begins to deviate from the observed line profile 2 Å from the line core. Such a deviation would be expected much nearer the line center where the line becomes optically thick. The wings are, however, extremely well fit by a highly broadened Doppler profile ( $\Delta\lambda_D = 3.5$  Å) which is blueshifted by  $\Delta\lambda_{bs} = 1.5$  Å. The width indicates a temperature of  $\sim 10^6$  K if thermal in origin, and a velocity of  $150 \text{ km s}^{-1}$  if microturbulent in origin. The blueshifted emitting material is rising at  $\sim 70 \text{ km s}^{-1}$ . Both the width and the blueshift persisted for 40<sup>m</sup> without varying before observing terminated. We note that the appearance of a central reversal in the  $H\alpha$  emission line profile during the flare, combined with the apparent inapplicability of Stark broadening to account for the line wings during outburst, is suggestive of a large flare emitting volume rather than a single, exceptionally high pressure, compact region as the site of flare  $H\alpha$  emission.

In brief summary, a qualitative picture of the flare would include upward moving material filling a large volume (i.e.,  $r \sim 0.1 R_*$ ) with hot plasma at chromospheric densities. The flare volume would produce line emission that is strongly enhanced in total flux compared to the

preflare emission but is otherwise similar in basic line profile shape to the profile in the quiescent chromosphere (aside from components that can be attributed to bulk motions in the line of sight).

The average white-light flare luminosity compared to the quiescent bolometric luminosity is  $\sim 3\%$ . This is an order of magnitude larger than the corresponding ratio for either chromospheric or coronal heating, or  $\sim 0.3\%$ . Hence, the conversion of flare energy to radiative flux is significantly more efficient than the processes that control coronal and chromospheric heating. This is not surprising given the dramatic increase seen in the chromospheric line emission spectrum. The energetics of the event can be accounted for within the context of two-ribbon flare models. Nevertheless, neither the actual flare morphology nor the true flare plasma heating mechanism are known in the case of stellar flare events.

We conclude that while these high resolution spectral observations are generally consistent with standard flare models discussed by Haisch (1989), they cannot be fit with simple one or two-dimensional models. Large stellar flares, like their solar counterparts, probably represent the superposition in space and time of many evolving flare regions in a flaring complex that could encompass a geometrically extended, large volume of emitting plasma.

We thank the Kitt Peak National Observatory and the Steward Observatory of the University of Arizona for the allocation of observing time for this project. We are grateful to T. Boroson for his assistance in the acquisition of the Reticon data, and to D. Rautenkranz for her assistance in the reduction of the Reticon scans. We acknowledge useful conversations with L. Cram and D. Neidig.

## REFERENCES

- Antonucci, E., & Dennis, B. R. 1983, *Recent Advances in the Understanding of Solar Flares*, edited by S. R. Kane (Reidel, Dordrecht), p. 67
- Baliunas, S. L., Avrett, E. H., Hartmann, L., & Dupree, A. K. 1979, *ApJ* 233, L129
- Bookbinder, J. A. 1985, Ph.D. thesis, Harvard University, Cambridge
- Bopp, B. W., & Moffett, T. M. 1973, *ApJ*, 185, 239
- Byrne, P. B. 1983, *Activity in Red Dwarf Stars*, edited by P. B. Byrne and M. Rodonò (Reidel, Dordrecht), p. 157
- Byrne, P. B. 1989, *Solar Phys.* 121, 61
- Byrne, P. B., & Rodonò, M. 1983, *Activity in Red Dwarf Stars*, edited by P. B. Byrne and M. Rodonò (Reidel, Dordrecht)
- Cram, L. E., & Woods, D. T. 1982, *ApJ*, 257, 269
- Gershberg, R. I. 1975, *Variable Stars and Stellar Evolution*, edited by V. E. Sherwood and L. Plaut (Reidel, Dordrecht), p. 47
- Giampapa, M. S. 1983, *Activity in Red Dwarf Stars*, edited by P. B. Byrne and M. Rodonò (Reidel, Dordrecht), p. 223
- Giampapa, M. S., Africano, J. L., Klimke, A., Parks, J., Quigley, R. J., Robinson, R. D., & Worden, S. P. 1982a, *ApJ* 252, L39
- Giampapa, M. S., Worden, S. P., & Linsky, J. L. 1982b, *ApJ*, 258, 740
- Gondhalekar, P. M. 1986, *Flares: Solar and Stellar*, RAL Workshop on Astronomy and Astrophysics, edited by P. M. Gondhalekar, RAL-86-085
- Gurzadyan, G. A. 1980, *Flare Stars* (Pergamon, Oxford)
- Haisch, B. M., et al. 1981, *ApJ*, 245, 1009
- Haisch, B. M., Linsky, J. L., Bornmann, P. L., Stencel, R. E., Antiochos, S. K., Golub, L., & Vaiana, G. S. 1983, *ApJ*, 267, 280
- Haisch, B. M., & Giampapa, M. S. 1985, *PASP*, 97, 340
- Haisch, B. M. 1989, *Solar Phys.*, 121, 3
- Haisch, B. M., & Rodonò, M. 1989, *Solar and Stellar Flares*, edited by B. M. Haisch and M. Rodonò (Kluwer, Dordrecht)
- Haisch, B., Strong, K. T., & Rodonò, M. 1991, *ARA&A*, 29, 275
- Kahn, S. M., Linsky, J. L., Mason, K. O., Haisch, B. M., Bowyer, C. S., White, N. E., & Pravdo, S. H. 1979, *ApJ*, 234, L107
- Kane, S. R. 1983, *Recent Advances in the Understanding of Solar Flares*, edited by S. R. Kane (Reidel, Dordrecht)
- Kopp, I., Lindgren, R., & Ryhd, B. 1974, *Table of Band Features of Molecules in Wavelength Order* (Institute of Physics, University of Stockholm)
- Kunkel, W. E. 1975, *Variable Stars and Stellar Evolution*, edited by V. E. Sherwood and L. Plaut (Reidel, Dordrecht), p. 15
- Lacy, C. H., Moffett, T. J., & Evans, D. S. 1976, *ApJS*, 30, 85
- Linsky, J. L., Bornmann, P. L., Carpenter, K. G., Wing, R. F., Giampapa, M. S., Worden, S. P., & Hege, E. K. 1982, *ApJ*, 260, 670
- Livshits, M. A., Badalyan, O. G., Kosovichev, A. G., & Katsova, M. M. 1981, *Solar Phys.*, 73, 269
- Mullan, D. J. 1977, *Solar Phys.*, 54, 183
- Mullan, D. J., & Tarter, C. B. 1977, *ApJ*, 212, 179
- Neidig, D. F. 1989, *Solar Phys.*, 121, 261
- Neidig, D. F., & Cliver, E. W. 1983, *Solar Phys.*, 88, 275

